A combined experimental and theoretical investigation of Cs$^+$ ions solvated in He$_N$ clusters

Ricardo Pérez de Tudela (iD), Paul Martini, Marcelo Goulart (iD), Paul Scheier (iD), Fernando Pirani (iD), Javier Hernández-Rojas (iD), José Bretón (iD), Josu Ortiz de Zárate, Massimiliano Bartolomei (iD), Tomás González-Lezana (iD), Marta I. Hernández (iD), José Campos-Martínez (iD), and Pablo Villarreal (iD)

View Online   Export Citation   CrossMark

ARTICLES YOU MAY BE INTERESTED IN

H$_2$, HD, and D$_2$ in the small cage of structure II clathrate hydrate: Vibrational frequency shifts from fully coupled quantum six-dimensional calculations of the vibration-translation-rotation eigenstates
The Journal of Chemical Physics **150**, 154303 (2019); https://doi.org/10.1063/1.5090573

Cs atoms on helium nanodroplets and the immersion of Cs$^+$ into the nanodroplet
The Journal of Chemical Physics **135**, 074306 (2011); https://doi.org/10.1063/1.3624840

A new full-dimensional ab initio intermolecular potential energy surface and vibrational states for (HF)$_2$ and (DF)$_2$
The Journal of Chemical Physics **150**, 154302 (2019); https://doi.org/10.1063/1.5090225

A combined experimental and theoretical investigation of Cs⁺ ions solvated in He$_N$ clusters

View Online   Export Citation   CrossMark

Ricardo Pérez de Tudela,[1] [iD] Paul Martini,[2] Marcelo Goulart,[2] [iD] Paul Scheier,[2] [iD]
Fernando Pirani,[3] [iD] Javier Hernández-Rojas,[4] [iD] José Bretón,[4] [iD] Josu Ortiz de Zárate,[5]
Massimiliano Bartolomei,[5] [iD] Tomás González-Lezana,[5,a] [iD] Marta I. Hernández,[5] [iD]
José Campos-Martínez,[5] [iD] and Pablo Villarreal[5] [iD]

AFFILIATIONS

[1]Lehrstuhl für Theoretische Chemie, Ruhr-Universität Bochum, 44780 Bochum, Germany

[2]Institut für Ionenphysik und Angewandte Physik, Universität Innsbruck, Technikerstr. 25, A-6020 Innsbruck, Austria

[3]Dipartimento di Chimica, Biologia e Biotecnologie, Universitá di Perugia, 06123 Perugia, Italy

[4]Departamento de Física and IUdEA, Universidad de La Laguna, La Laguna, 38205 Tenerife, Spain

[5]Instituto de Física Fundamental, IFF-CSIC, Serrano 123, 28006 Madrid, Spain

a)Electronic mail: t.gonzalez.lezana@csic.es

ABSTRACT

Solvation of Cs⁺ ions inside helium droplets has been investigated both experimentally and theoretically. On the one hand, mass spectra of doped helium clusters ionized with a crossed electron beam, He$_N$Cs⁺, have been recorded for sizes up to $N = 60$. The analysis of the ratio between the observed peaks for each size N reveals evidences of the closure of the first solvation shell when 17 He atoms surround the alkali ion. On the other hand, we have obtained energies and geometrical structures of the title clusters by means of basin-hopping, diffusion Monte Carlo (DMC), and path integral Monte Carlo (PIMC) methods. The analytical He–Cs⁺ interaction potential employed in our calculations is represented by the improved Lennard-Jones expression optimized on high level *ab initio* energies. The weakness of the existing interaction between helium and Cs⁺ in comparison with some other alkali ions such as Li⁺ is found to play a crucial role. Our theoretical findings confirm that the first solvation layer is completed at $N = 17$ and both evaporation and second difference energies obtained with the PIMC calculation seem to reproduce a feature observed at $N = 12$ for the experimental ion abundance. The analysis of the DMC probability distributions reveals the important contribution from the icosahedral structure to the overall configuration for He$_{12}$Cs⁺.

Published under license by AIP Publishing. https://doi.org/10.1063/1.5092566

I. INTRODUCTION

Helium droplets are considered as an ideal environment for spectroscopical investigations of different species.[1–7] Among all possible impurities to dope the He$_N$ clusters, alkali ions have received special attention in recent studies.[8–24] From the experimental side, for instance, Müller *et al.*[25] performed a systematic study of the formation and stability of snowballs obtained by femtosecond photoionization of small alkali clusters bound to helium nanodroplets. The authors concluded that the size of the doped helium cluster depends on the mass of the alkali atom: whereas for Na⁺ and K⁺ ions, clusters between 3 and 10 He atoms were observed, the

heavier alkali Rb⁺ and Cs⁺ led to the formation of snowballs containing up to 41 He atoms. Differential mass spectra obtained as abundance mass ratios of neighboring snowball intensities, I_{N+1}/I_N, as a function of the number of He atoms, N, were analyzed in order to characterize the structure of the cluster around the ionic impurity. In particular, indications of shell closures of the solvating atoms were inferred from dips observed in such relative intensities. The drop found in the spectra for He$_N$Cs⁺ at $N = 16$ is slightly shifted with respect to the theoretical prediction reported by Rossi *et al.*,[26] who calculated $N = 17.5$ by numerical integration of the radial density profile obtained in a shadow Monte Carlo (MC) calculation. The authors suggested the existence of another relatively stable

structure at $He_{12}Cs^+$ to explain the additional dip featured by the differential intensity at $N = 12$[25] and referred to the classical lowest energy configuration seen for $He_{12}K^+$ in the calculations reported in Ref. 27. The immersion of Cs^+ into the He_N nanodroplets was also experimentally investigated by Theisen *et al.*,[20] and the only deviations from a smooth dependence of the photoion yield with respect to N were observed around $N = 17$–18 and $N = 50$. Both features were associated, in principle, to shell closures (first and second shell, respectively) although, due to its non rigid character, the exact number filling a second layer surrounding the ionic impurity could fluctuate.

Previous theoretical investigations of He_NCs^+ in the literature found a structure consisting of the ion localized at the center of a droplet formed by surrounding He atoms in a snowball along well defined shells.[26,28,29] Galli *et al.*[29] performed path integral Monte Carlo (PIMC) calculations of these systems at $T = 1$ K in comparison with ^{4}He nanodroplets doped with some other alkali and alkali-earth ions such as Na^+, K^+, Be^+, and Mg^+. Density profiles of helium atoms around the Cs^+ ion were calculated for different sizes N. The number of He atoms in the first shell changed from 17 for $He_{20}Cs^+$ up to 18 when the calculation was performed for $He_{64}Cs^+$ and $He_{128}Cs^+$. The radial probability densities displayed different peaks associated with the filling of shells around the cesium ion as more helium atoms are added to the cluster. In particular, the authors of Ref. 29 saw that the second maximum at ~6 Å is characterized by He atoms with high radial mobility which can participate in position changes with atoms of the first shell, in agreement with conclusions reported in Ref. 28.

In a recent experiment,[30] helium nanodroplets doped with cesium in the presence of molecular hydrogen were subsequently ionized with a crossed electron beam. The obtained mass spectra were analyzed in order to study mainly the abundance of $(H_2)_NCs^+$. The most prominent mass peaks were due, however, to the existence of He_NCs^+ clusters. The corresponding ion abundance curve as a function of the number of He atoms was shown for sizes smaller than $N = 30$, revealing just a suggested feature around $N = 15$.[30]

In this work, we present results for a similar experiment performed only with cesium atoms in the pickup chamber in an attempt to obtain much clearer conditions for a proper inspection of the relative abundances of the different Cs^+ ions solvated with helium atoms. In addition to this and in order to search for the most stable configurations, we have carried out extensive theoretical calculations by means of both classical and quantum mechanical (QM) approaches. In particular, basin-hopping (BH), diffusion Monte Carlo (DMC), and PIMC calculations have been performed in comparison with the new experimental data. Analogously as in previous theoretical investigations of similar clusters (see, for instance, Ref. 31 for the case of He_NLi^+), our study includes the explicit *ab initio* calculation of the $He–Cs^+$ interaction which has been used to optimize an analytical representation according to an improved Lennard-Jones (ILJ) expression.

The structure of the paper is the following: Details of the experimental setup are given in Sec. II; the potential energy surface (PES) is described in Sec. III; details of the theoretical methods employed in our calculations are shown in Sec. IV. Results are shown and discussed in Sec. V and Sec. VI, respectively, and finally, conclusions are given in Sec. VII.

II. EXPERIMENTAL DETAILS

Helium nanodroplets were produced by expanding helium (Linde, purity 99.9999%) at a stagnation pressure of about 2.6 MPa through a 5 μm nozzle, cooled by a closed-cycle cryostat (Sumitomo Heavy Industries Ltd., model RDK-415D), into vacuum. The nozzle temperature was set to 9.9 K, resulting in an average droplet size of about 5×10^5 He atoms.[23,32] The resulting supersonic beam was confined by a 0.8 mm conical skimmer, located 8 mm downstream from the nozzle, and passed through a 20 cm-long differentially pumped chamber. The droplets crossed through a pick-up cell filled with cesium vapor produced in a resistively heated oven. The temperature of the metal oven was set to 327.5 K. The doped helium nanodroplets passed through another differentially pumped vacuum chamber where they were crossed with an electron beam of 85 eV energy. The emission current was 46 μA. Ions were guided by electrostatic lenses into the extraction region of a commercial orthogonal time-of-flight (TOF) mass spectrometer equipped with a reflectron (Tofwerk AG, model HTOF). The effective mass resolution was $m/\Delta m = 5400$ (Δm = full-width-at-half-maximum). The ions were detected by a micro-channel plate operated in single ion counting mode and recorded via a time to digital converter. Additional experimental details have been described elsewhere.[33] The mass spectrum was evaluated by means of a custom-designed software.[34] The program corrects for experimental artifacts such as background signal levels, imperfect peak shapes, and mass drift in case of long-term measurements.

III. POTENTIAL ENERGY SURFACE

Pairwise two-body (2B) functions have been employed to describe the He–He and He–Cs^+ interactions. In particular, for He–He, we have used the potential reported in Ref. 35, whereas for the He–Cs^+ contribution, a new potential energy surface (PES) optimized on accurate coupled-cluster with single and double and perturbative triple excitations [CCSD(T)] interaction energies obtained with the d-aug-cc-pV6Z[36] and def2-AQVZPP[37] basis sets for He and Cs^+, respectively, has been developed. We have checked that the adopted basis set is sufficiently large to guarantee well converged interaction energies, which are found to deviate from those carried out in the global minimum region with the d-aug-cc-pV5Z/def2-AQVZPP set of less than 0.3 meV (about 1%). The CCSD(T) computations have been performed using the Molpro2012.1 package.[38] For the analytical representation of the force field, the ILJ formulation[39] of the atom-atom interactions has been chosen

$$V(r) = \epsilon \left[\frac{m}{n(r) - m} \left(\frac{r_m}{r} \right)^{n(r)} - \frac{n(r)}{n(r) - m} \left(\frac{r_m}{r} \right)^m \right]. \quad (1)$$

In the expression above, ϵ is the potential depth, r_m is the minimum potential position, and $n(r)$ is defined as follows:[39]

$$n(r) = \beta + 4 \left(\frac{r}{r_m} \right)^2. \quad (2)$$

Values for the parameters used in Eqs. (1) and (2) are shown in Table I.

Both the *ab initio* points and the analytical representation for the He–Cs^+ interaction potential are shown in Fig. 1 besides the

TABLE I. Parameters for the ILJ potentials employed for the He–Cs$^+$ interaction shown in Eqs. (1) and (2). r_m is given in Angstrom, ϵ is given in milli electron volt; m, and β are dimensionless parameters.

m	r_m	ϵ	β
4	3.35	13.70	9.5

He–He potential taken from Ref. 35. The comparison with the He–Li$^+$ case, a system formed with a much lighter alkali ion treated in a previous investigation,[31] reveals the weak character of the existing interactions responsible for the stability of the Cs$^+$ doped helium clusters. As shown in Fig. 1, the He–Li$^+$ interaction is about 5 times deeper than the He–Cs$^+$. The reason has to be found in the different charge distribution of each ion. Due to the smaller size of Li$^+$, the charge of the ion is distributed in a shorter and more compact region, so the He atoms are capable to penetrate closer to the impurity. Cs$^+$ is, on the contrary, bigger, and the charged electronic cloud extends therefore at a further distance with respect to the center. The rare gas atoms can not get close to the impurity thus resulting in a weaker interaction shifted at larger interatomic distances.

IV. THEORETICAL METHODS

A. Basin-hopping

Putative global energy minima of He$_N$Cs$^+$ clusters with $N \leq 30$ were located using the BH method[40] also known as the "Monte Carlo plus energy minimization" approach of Li and Scheraga.[41] This unbiased technique has been particularly successful for the global optimization of various atomic and molecular systems.[42–50] The BH method relies on an extensive random search of the PES by
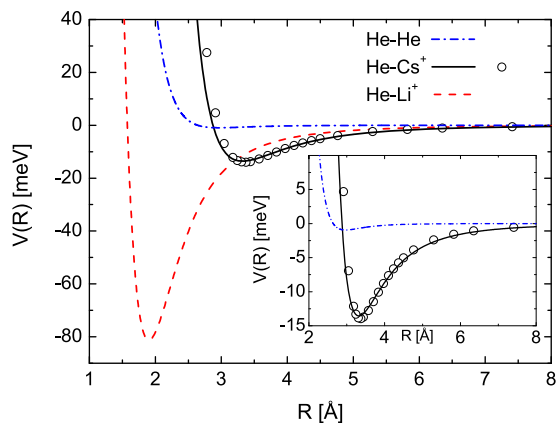

FIG. 1. Potential energy curves for He–Cs$^+$ (in circles *ab initio* points and in the black solid line the ILJ analytical fit) and He–He[35] (in the blue dashed-dotted line) interactions employed in this work. The He–Li$^+$ case (red dashed line) from Ref. 31 has been included for comparison in the bigger panel, while in the inset, the He–He and He–Cs$^+$ cases are shown in a more reduced range.

large amplitude MC moves followed by systematic local optimization. Suitable parameters for the present BH simulations were determined for all cluster sizes based on preliminary tests on He$_{12}$Cs$^+$. These benchmarks consisted of 10^5 minimization steps and were initiated from independent random geometries, varying the temperature and the target acceptance ratios of the MC simulation. Although our global minima remain putative, they were obtained in all trajectories. This should ensure a reasonably high degree of confidence.

The results below were obtained at a constant simulation temperature of $k_B T = 2$ meV (where k_B is the Boltzmann constant) and an acceptance ratio of 50%. A total of 4 runs of 5×10^5 BH steps each were performed for all sizes. The quantum effects were included through the zero-point energy (ZPE) function, in the harmonic approximation.[31,51,52] To do it, we built a database of local minima close to the global minimum for each cluster size. In some cases, the geometry of the BH+ZPE global minimum differs from the BH one.

B. Diffusion Monte Carlo

DMC[53,54] calculations are carried out by propagating in imaginary time ($\tau = it$) a time dependent Schrödinger equation, in such a way that the general solution,

$$\Psi(\tau) = \sum_n c_n \, \psi_n \, e^{-\tau E_n / \hbar}, \quad (3)$$

will lead, in the long-time limit, to only one non-vanished term that will correspond to E_0, the ground state energy.

Depending on the cluster size and therefore the number of He atoms, the number of replicas included are within the range 6000–12 000, with typical time steps $\Delta\tau = 40$–80 a.u., over 4000–8000 time steps and using descendant weighting with 6–9 generations.

C. Path integral Monte Carlo

The PIMC method employed in this work has been described before several times,[31,51,52,55–58] so here we will only discuss the most relevant details of the calculation. The density matrix of the system at a temperature T is expressed as the product of densities at temperature $T' = T \times M$ and is evaluated in a collection $\mathcal{R}_\alpha \equiv \{\mathbf{r}_1^\alpha, \ldots, \mathbf{r}_N^\alpha\}$ of position vectors $\mathbf{r}_i^\alpha$ of the particles forming the cluster. The α index runs over the M quantum beads or time slices.

The total energy of the Cs$^+$ doped helium clusters can be obtained by means of the so-called virial estimator[59,60] expressed as

$$\langle E(T) \rangle = \frac{3N}{2\beta} - \left\langle \frac{1}{2M} \sum_{\alpha=1}^M \sum_{i=1}^N (\mathbf{r}_i^\alpha - \mathbf{r}_i^C) \cdot \mathbf{F}_i^\alpha \right\rangle + \left\langle \frac{1}{M} \sum_{\alpha=1}^M V(\mathcal{R}_\alpha) \right\rangle, \quad (4)$$

where $\mathbf{r}_i^C = M^{-1} \sum_{\alpha=1}^M \mathbf{r}_i^\alpha$ defines the centroid of the M beads and $\beta = (k_B T)^{-1}$. The first term in Eq. (4) corresponds to the classical kinetic energy after substracting the center of mass degrees of freedom; the second one is a quantum correction where $\mathbf{F}_i^\alpha$ is the force experienced by the i-particle on the α slice and the third term describes the interaction between each pair of particles on that α slice according with the pairwise interactions described in Sec. III. The Cs$^+$ ion is located fixed at the origin, and it is not included

in the calculations, which are exclusively for the He atoms. This is an acceptable approximation given its large mass in comparison with He. The rigidity of the clusters is investigated by means of the Lindemann index, defined as follows:[51,61]

$$\delta_i = \frac{1}{M(N-1)} \sum_{\alpha=1}^{M} \sum_{j \neq i}^{N} \frac{\sqrt{\langle r_{ij}^{\alpha 2} \rangle - \langle r_{ij}^{\alpha} \rangle^2}}{\langle r_{ij}^{\alpha} \rangle}, \quad (5)$$

where $r_{ij}^{\alpha} = |\mathbf{r}_i^{\alpha} - \mathbf{r}_j^{\alpha}|$ is the He–He distance at the time slice α. Moreover, our analysis includes the calculation of the so-called radius of gyration (ROG), obtained as follows:

$$(R_g)_i = \sqrt{\frac{1}{M} \sum_{\alpha=1}^{M} (\mathbf{r}_i^{\alpha} - \mathbf{r}_i^{C})^2}, \quad (6)$$

which measures the quantum delocalization of each individual atom. The PIMC calculation is performed at $T = 2$ K using $M = 200$ beads. The integration of the above terms shown in Eq. (4) is carried out via a Metropolis MC algorithm averaging over a number of paths $\{\mathcal{R}_1, \mathcal{R}_2, \ldots, \mathcal{R}_M, \mathcal{R}_{M+1}\}$ sampled by means of a staging procedure[62] moving about 10% (that is 20) of the beads. About $10^6 \times N$ staging moves for thermalization and about $10^7 \times N$ for statistics were considered. A confinement procedure was employed to avoid the evaporation of the He atoms beyond a cut-off radius defined by inspection of radial probability density functions.

V. RESULTS

A. Experimental results

Integrated counts from the $He_N Cs^+$ complexes have been obtained as a function of the number of He atoms, N, as in previous investigations for similar systems.[10,30,31] The ion intensities, shown in Fig. 2 for complexes up to $N = 60$, exhibit a mainly structureless profile with the only exception of a drop after $N = 12$ and a soft shoulder between $N = 14$ and 18. In principle, one may
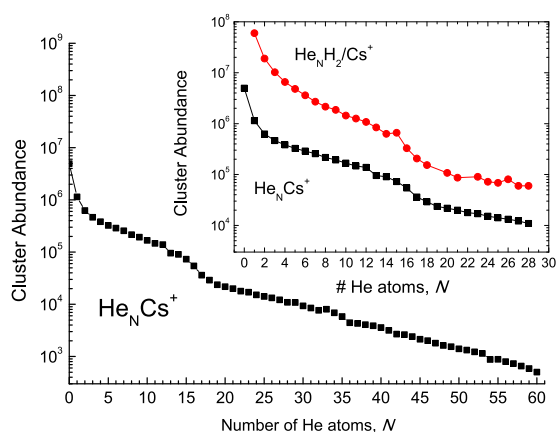
relate both anomalies to a stable structure for $He_{12}Cs^+$, perhaps an icosahedral arrangement as suggested for $He_{12}Kr^+$,[27] and to possible indications of complete filling of the first shell, respectively. Much more smoother features are suggested at larger sizes, about $N = 33–35$ and $N = 53$. In the inset of Fig. 2, the present ion mass abundance is compared for $N \leq 28$ with that reported in the recent study by Kranabetter et al.[30] of helium nanodroplets doped not only with Cs^+ but also with H_2. The comparison between the curves shown in Fig. 2 reveals that the small peak at $N = 15$ in the case of the $He_N Cs^+$ experiment (red circles in Fig. 2) is not seen in this work, where no H_2 is introduced in the pick-up chamber besides helium and cesium. The feature observed in Ref. 30 has its origin in a double peak at $m/z \sim 193$ assigned both to $He_{15}Cs^+$ and a fragment of a polydimethylsiloxane, $S_3C_3H_9O_4^+$, used as a lubricant for turbo pumps. Once this additional contribution is removed after extended baking, no intensity anomaly for $He_{15}Cs^+$ is found and the cluster abundance does not exhibit a suggested peak at $N = 15$ (see Fig. 2).

Two portions of the mass spectrum recorded after electron ionization of the Cs doped helium nanodroplets are shown in Fig. 3 at the mass per charge range corresponding to the regions between $He_{14}Cs^+$ and $He_{16}Cs^+$ and close to $He_{26}Cs^+$. Besides these contributions from the Cs^+ doped clusters, peaks for He_N^+ with $N = 47–49$ and 59, respectively, are also observed. As already reported in Ref. 23, all He_N^+ ions exhibit a narrow satellite peak (indicated with vertical arrows in Fig. 3) next to their nominal mass, typically 0.1–0.3 amu upshifted. For the $He_N Cs^+$ cluster, on the contrary, this extra peak is seen only for $He_{26}Cs^+$ but seems to be absent for $N = 14–16$. As reported in Ref. 63, these extra features close to the main peaks originate from metastable decay of cluster ions on their way through the TOF mass spectrometer. They can be understood as indications of unimolecular dissociation of the type

FIG. 2. Measured abundances of $He_N Cs^+$ as a function of the number of He atoms, N, up to $N = 60$. In the inset, present results (black squares) are compared for $N \leq 28$ with previous measurements (red circles) obtained in an experiment performed with helium nanodroplets doped with cesium and molecular hydrogen.[30]
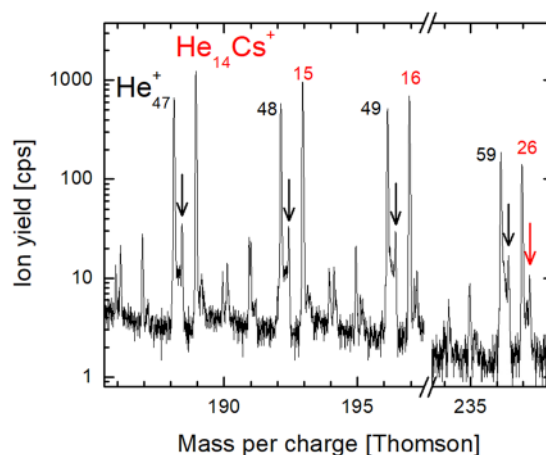

FIG. 3. Section of the mass spectrum obtained by electron ionization of Cs doped Helium nanodroplets. Conditions: electron energy 85 eV, electron current 46 μA, helium temperature 9.9 K, and He pressure 2.6 MPa. In this semilogarithmic plot, all pristine helium cluster ions and the $He_{26}Cs^+$ maximum peak exhibit a satellite peak (indicated by arrows) upshifted by about 0.3 Thomson and about 5% of the intensity of the main peak which can be assigned to fragmentation processes in the ion extraction region of the TOF mass spectrometer.

$He_{N+1}Cs^{+*} \rightarrow He_NCs^+ + He$ or a tightly bound He_3^+ core[64] in the field free region before entering the reflectron. These satellite peaks are particularly strong for weakly bound cluster ions and their relative position compared to the parent, and promptly formed fragment ion depends strongly on the settings of the reflector voltage (see Fig. 13 in Ref. 63).

A detailed analysis for the entire spectrum (not shown here) reveals that the relative intensity of the satellite peaks (relative to the main peaks) increases from $<10^{-3}$ for $N = 1$ to more than 10% for $N > 100$. As shown in Fig. 4, where we plot such a ratio both for He_NCs^+ (up to $N = 26$) and He_N^+ clusters (between $N = 33$ and $N = 60$), there is a substantial increase beyond $He_{17}Cs^+$. Pronounced changes in the slope (as those seen in Fig. 4) indicate shell closures due to the presence of more weakly bound He atoms occupying the next solvation layer. Our present result would thus be consistent with previous theoretical reports of 17.5 as the number of He atoms in the first shell.[26]

B. Theoretical results

The energy per particle for the He_NCs^+ clusters here investigated has been analyzed as a function of the droplet size. The results obtained by means of the BH approach shown in Fig. 5 reveal an interesting change as N increases. Beyond $N = 17$, the slope of the energy curve changes its behavior with respect to N and becomes positive. A similar effect was observed in the study of the solvation of K^+ in helium droplets performed by Yurtsever et al.[22] In that case, authors found that the minimum observed for $He_{12}K^+$ clusters corresponds to a specially stable symmetric structure of the helium atoms around the ion impurity located at the center. The features observed in the trend of the E/N curve calculated with the BH method shown in Fig. 5 can be associated with specific configurations of the He atoms around the Cs^+ ion obtained by means of classical approaches.[43] Thus, for instance, that minimum seen for the case of $He_{17}Cs^+$ corresponds to an optimum packing structure, that is, the configuration in which the He atoms covers in the most optimum way the Cs^+ ion, providing the lowest association energy
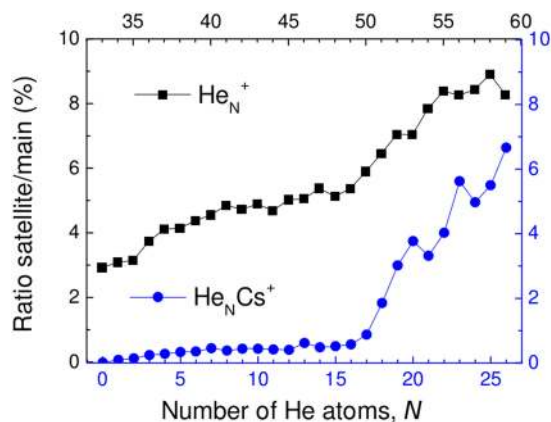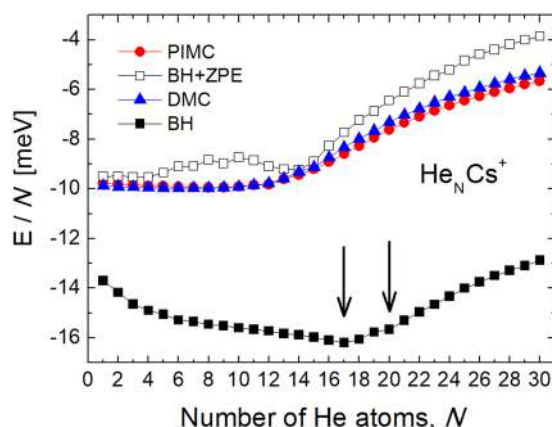

FIG. 5. Energy per particle for the He_NCs^+ clusters as a function of the number of He atoms, N, obtained by means of the BH (black solid squares), PIMC (red circles), DMC (blue triangles), and BH+ZPE (empty squares). Units are milli electron volt. The $N = 17$ and 20 cases, corresponding to the optimum and maximum packing structures, respectively, are highlighted with the vertical arrow in the BH results. See text for details.

per atom. The corresponding structure, presented in the left panel of Fig. 6, belongs to the D_{5d} symmetry point group.

A further analysis of the BH results of Fig. 5 reveals a second feature at a slightly larger size, $N = 20$, where the energy per particle curve displays a local minimum. The corresponding structure found in the classical minimization procedure is shown in the right panel of Fig. 6. It belongs to the C_1 symmetry point group and can be interpreted as the maximum packing structure in which the system supports a supplementary number of atoms with a slight raise of the cluster association energy per atom.[43]

The corresponding QM estimates of the energies per particles shown in Fig. 5 exhibit, however, a different behavior as a function of the cluster size. Both the PIMC and DMC results display a change with a pronounced increase in the slope of the energy curve beyond $N \sim 12$. The maximum value of the first derivative of the $E/N(N)$ curve is seen around $N = 18$ in both cases. The QM corrected value of the BH energies obtained adding the ZPE values,

FIG. 4. Ratio between satellite and the main peak for He_N^+ from $N = 33$–59 (black) and for He_NCs^+ ions with N between 0 and 26 (blue).

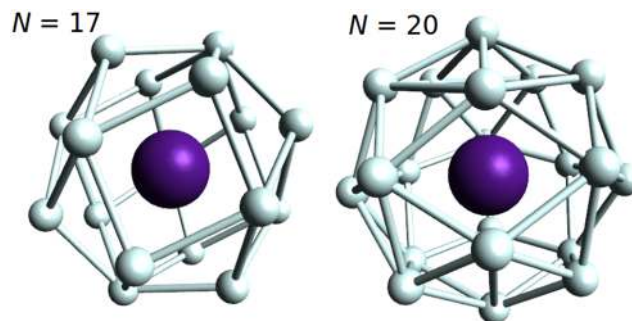**FIG. 6**. Minimum energy structures obtained with the BH method for the $He_{17}Cs^+$ and $He_{20}Cs^+$ cases. These are the optimum and maximum packing structures, respectively, marked in Fig. 5 with the vertical arrow (see text for details).

BH+ZPE, shows a much more fluctuating trend at the small and medium sizes, with values which significantly differ from the DMC and PIMC counterparts between $N = 4$ and 14.

The PIMC energies have been obtained using a confinement approach as explained in Sec. IV C. As opposed to what is stated in Ref. 29, where the corresponding PIMC calculation is performed at 1 K, the binding of the He atom to the Cs ion does not seem to be enough to prevent evaporation from the cluster when the temperature is increased up to 2 K as in our study. In Fig. 7, we compare the behavior of the $He_N Cs^+$ total energies calculated with the PIMC approach with and without such an artificial restriction for the He atoms as a function of N. It is clear that this procedure is only necessary beyond $N = 18$ since for smaller sizes, both calculations lead to essentially the same values of the energies. However, when more He atoms are added, the PIMC calculation with no confinement yields fluctuating energies (see the inset of Fig. 7 for an amplified view of that range of cluster sizes).

The onset of this behavior at $N = 18$ seems to be related with the closure of the first solvation layer of helium atoms surrounding the Cs ion. As a matter of fact, if we calculate the radial probability density functions for the $He_N Cs^+$ clusters with $N = 16$, 18, 25, and 27 (shown in Fig. 8), we can see how $He_{18} Cs^+$ is the first case in which, besides a main maximum around ~3.5 Å, a secondary peak starts to develop around ~6 Å. For $N = 25$ and 27, this feature is well defined thus indicating the relative position of those He atoms occupying a second layer when $N \geq 18$. These two maxima are also seen in the PIMC calculation reported by Galli et al.[29] for $He_{128} Cs^+$ in addition to an extra peak at even larger distances (~9 Å), a region which remains, however, unexplored in our present case with a remarkably lower number of He atoms.

Similar fluctuations are seen when we calculate the evaporation energy, defined as $\Delta E_N = -[E_N - E_{(N-1)}]$. The BH results, compared with DMC, PIMC, and BH+ZPE values in Fig. 9, display a stable character with the number of helium atoms up to $He_{17} Cs^+$, when a noticeable decrease is observed. The other significant feature seen in the trend followed by ΔE_N obtained by means of the BH approach

FIG. 8. Radial probability distribution obtained with the PIMC method for $He_N Cs^+$ clusters with $N = 16$ (black), 18 (red), 25 (blue), and 27 (magenta).

occurs at $N = 19$, that is, at the strict vicinity of the maximum packing structure seen for $N = 20$ (see Fig. 6). Beyond that point, the classical predictions remain almost stable as the size of the cluster increases.

The analysis of the evaporation energies obtained by means of the QM methods here employed reveals the difficulty of the calculation due to the extreme weakness of the interaction between the He and Cs^+. The PIMC results at $T = 2$ K shown in Fig. 9 have been calculated with the artificial confinement mentioned in Sec. IV C to avoid the evaporation of He atoms from the cluster. As seen in Fig. 7, this procedure seems to be crucial to eliminate spurious fluctuations in the energy of the Cs^+ ion doped clusters at such temperature. This explains the plateau observed as N increases for the evaporation energies in Fig. 9. In this sense, our results manifest the substantial effect due to the temperature in the system, in comparison with the non-restricted PIMC calculation performed at $T = 1$ K reported in Ref. 29. Analogously, the DMC approach yields
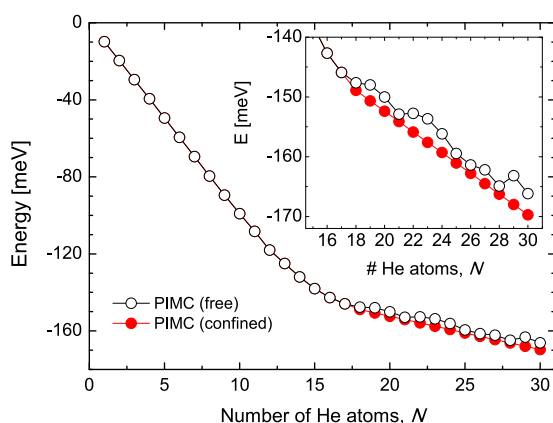

FIG. 7. Energies for the $He_N Cs^+$ clusters (with N between 1 and 30) obtained by means of the PIMC method of Sec. IV C. Results obtained when He atoms are free to move (open circles) are compared with those energies calculated with a confinement procedure (red circles). See text for details.
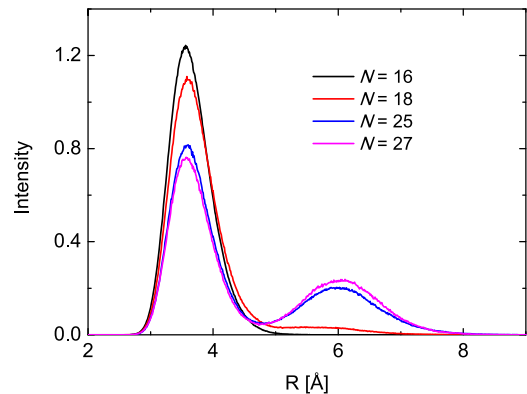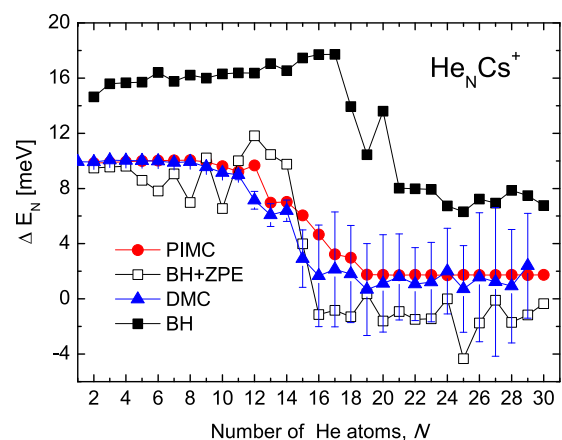

FIG. 9. Evaporation energies as a function of N, the number of He atoms, $\Delta E_N = -[E_N - E_{(N-1)}]$ for the $He_N Cs^+$ clusters as a function of the number of He atoms, N, obtained with the BH (black solid squares), PIMC (red circles), DMC (blue triangles), and BH+ZPE (empty squares). Units are milli electron volt.

energies with considerable fluctuations with respect to N and large error bars when the clusters become sufficiently large, so peaks seen in the evaporation energy curve beyond $N > 20$ in Fig. 9 should be taken cautiously. For the smaller clusters, $N \leq 15$, however, the PIMC and DMC energies compare well. The ZPE corrected BH predictions struggle to provide stable values of the energies at almost all sizes. Possible deviations from the harmonic approximation and the proximity of various shallow potential energy wells seem to be the most likely reasons for such poor performance to describe correctly the energy landscape for the He_NCs^+ clusters here investigated.

With these considerations in mind, we only employ the PIMC with the confinement restriction to calculate the second energy differences, that is $\Delta_2 E_N = E_{N+1} - E_{N-1} - 2E_N$, another commonly employed descriptor to analyze cluster stability.[31,65] The dependence of such $\Delta_2 E_N$ as a function of N, shown in Fig. 10, reveals also a prominent peak for $He_{12}Cs^+$, supporting the above discussed findings for the evaporation energies. The region of the closure of the first solvation shell is also affected by noticeable features since a pronounced dip for $N = 17$ is immediately followed by a maximum at $N = 18$.

Indications of a possible change in the overall behavior of the He_NCs^+ clusters when the number of helium atoms is increased, can be additionally analyzed by means of both the Lindemann index and ROG defined in Eqs. (5) and (6), respectively. In Fig. 11, we show both quantities as a function of N in order to see if He atoms exhibit distinct behavior individually for each cluster size. In particular, the values of δ_i for the He atoms (see the top panel of Fig. 11) in $He_{12}Cs^+$ display a noticeable decrease with respect to the trend followed by smaller clusters and a change in the slope of the curve at $N = 18$. These are precisely the two specific sizes at which the experiment has found a distinctive behavior. In principle, values of the Lindemann index are above $\delta_i \sim 0.2$, thus indicating a well-developed fluid behavior[61] for the entire range of sizes investigated here. It is also significant that, as the number of He atoms in cluster is increased, such trend augments with a tendency to stabilize around $\delta_i \sim 0.35$.
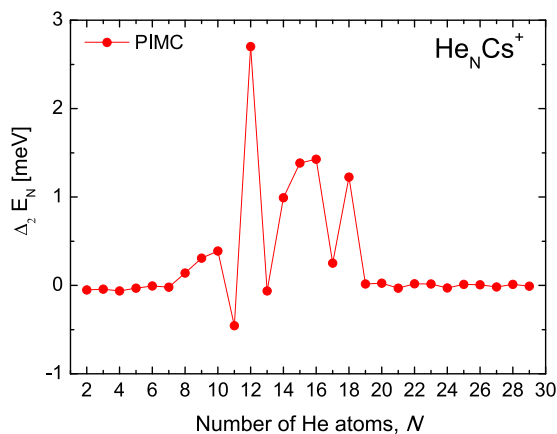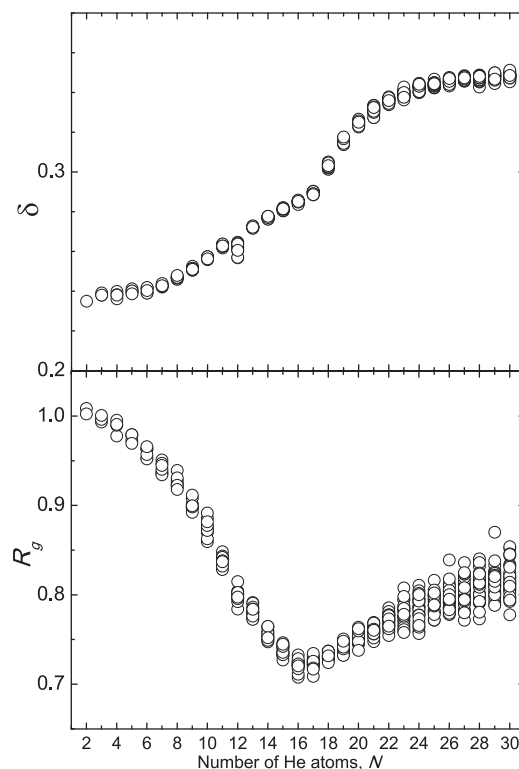
FIG. 11. Lindemann index δ_i for each He atom as defined in Eq. (5) and ROG, R_g, defined in Eq. (6) for the He_NCs^+ clusters as a function of the number of helium atoms, N, obtained with the PIMC method.

The ROG shown in the bottom panel of Fig. 11 exhibits a decreasing behavior as a function of N with a clear minimum for the region around $He_{16}-Cs^+$ and $He_{17}Cs^+$, and then it starts increasing again. Beyond that point, although there is certainly some spread of the He atoms location with values of R_g covering an ampler range, no separated groups are observed thus suggesting no significant differences between the behavior at the first and second solvating helium layers. The decrease observed with N is an indication of the increase in He–He interactions as the size of the cluster keeps increasing. For larger values of N there is a wider variety of possible ROG for each cluster size.

VI. DISCUSSION

The drop at $N = 12$ seen in the experimental cluster abundance shown in Fig. 2 has a correspondence in the QM evaporation energies (see Fig. 9). According to the predictions obtained with the PIMC approach, $He_{12}Cs^+$ is the largest cluster with a value for $\Delta E \sim 10$ meV. The addition of another He atom produces a significant decrease in the evaporation energy down to ~6 meV. However, there is nothing in the radial probability density obtained with such a method which may indicate a special configuration for this cluster. Analogously, the related minimum energy configuration predicted by the BH approach corresponds to a structure where the He atoms do not even completely solvate the Cs^+ ion thus

FIG. 10. Second energy differences defined as $\Delta_2 E_N = E_{N+1} - E_{N-1} - 2E_N$ calculated with the PIMC method.

providing no indication at all of significant stability. The angular distribution obtained by means of the DMC approach, however, suggests that the structure of $He_{12}Cs^+$ explores the icosahedral arrangement. Figure 12 shows the comparison between the $He–Cs^+–He$ angle distribution for $N = 12$ and that from the hypothetical case in which He atoms form a strict icosahedral around the Cs^+ ion. Both distributions are far from being identical, but one can infer the presence of this stable configuration on the overall distribution of the cluster. A bit more conclusive seems the comparison of the corresponding probability distributions for the He–He and $He–Cs^+$ distances shown in Fig. 13. Apart from some slight shift in the maximum peak, the distribution for the distance between the He atoms and the Cs^+ ion obtained with the DMC calculation and that from the icosahedral structure are almost the same. The He–He distribution, on the other hand, exhibits a bimodal profile in which the second broad maximum seems to account for the distance separating the most distant He atoms: (i) He atoms in opposite vertices and (ii) a He atom in the vertex and those five from the most distant pentagon. Thus, although the energy per particle function of Fig. 5 does not have a minimum for such cluster size, $He_{12}Cs^+$ plays the role of the optimum packing structure in the QM case, which is classically seen for $He_{17}Cs^+$ (see Fig. 6).

The experimental cluster abundance shown in Fig. 2 displays a significant feature at $N = 17$. As suggested in previous studies and conclusively confirmed with the present calculations, this is precisely the number of He atoms required to fill the first solvation shell around the Cs^+. It is worth remarking that the satellite/main ratios shown in Fig. 4 constitute, up to our knowledge, the first experimental evidence of the closure of that first layer. According to the theoretical results reported in Ref. 29, the radial He density for $He_{64}Cs^+$ displays some non-negligible probability beyond that second peak around ~6 Å thus suggesting that He atoms start to explore a region outside a second layer, but a clear extra peak (around ~9 Å) is only seen for the distribution corresponding to $N = 128$. The present experimental investigation,
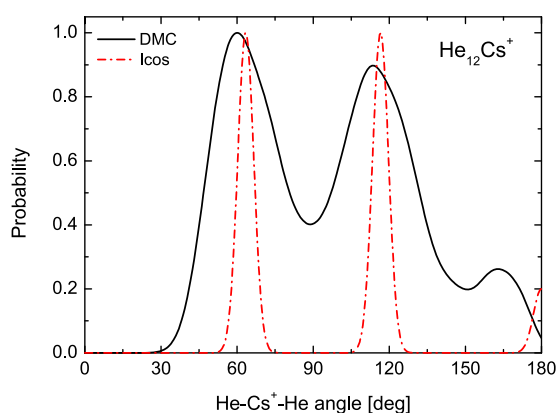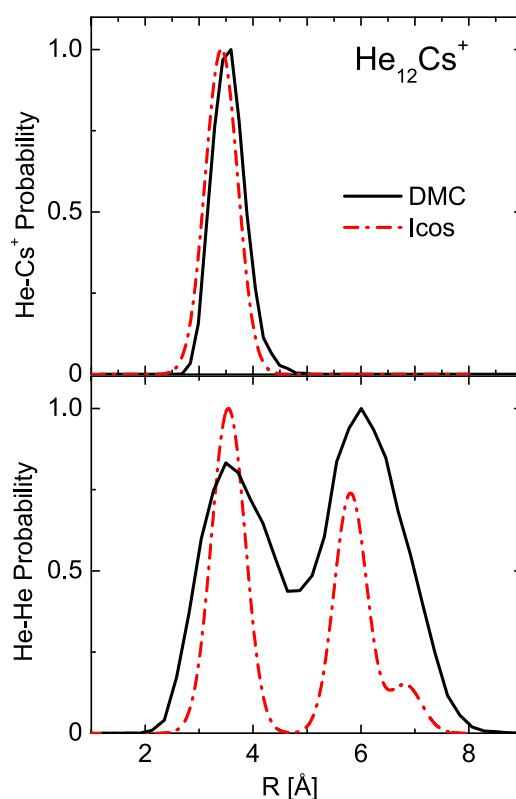
FIG. 13. Probability density functions for the $He–Cs^+$ (top panel) and He–He (bottom panel) distances obtained by means of the DMC method (black solid line) for the $He_{12}Cs^+$ cluster. As in Fig. 12 for the angular case, the radial distributions for a strict icosahedral structure (red dashed line) are included for comparison.

restricted to lower sizes, $N \leq 60$, can not give any insight about the closure of a second shell around the Cs^+ ion for such large clusters.

As mentioned in Sec. V B, the weak interaction existing between the He atoms and the Cs^+ ion makes the theoretical study of these clusters a challenging task. This specific condition is also manifested in previous investigations of similar doped helium droplets in which Cs^+ was comparatively treated with some other alkali ion impurities such as Li^+, Na^+, or K^+.[26,28] Thus in the variational MC calculation of Ref. 28, contrary to results for the other lighter ions, $He_N–Cs^+$ was the only case in which a not well defined shell of helium atoms surrounding the impurity was found. In addition, the angular correlations around Cs^+ were less defined than those around Li^+, Na^+, or K^+. In our case, $T = 2$ K seems to be a sufficiently high value of the temperature for the PIMC calculation (in comparison with previous investigations performed at $T = 1$ K[29]) to require the use of a confinement procedure to ensure converged results with no evaporation of He atoms from the droplet. Otherwise, the obtained results display spurious fluctuations as a function of the cluster size. The mainly structureless profile obtained for the evaporation energy as N increases seems to be consistent with the experimental result. Oscillations with the cluster size, so avoided in the case of the PIMC calculation, are on the contrary present in results obtained with

FIG. 12. Probability density function for the $He–Cs^+–He$ angle obtained by means of the DMC method (black solid line) for the $He_{12}Cs^+$ cluster. The angular distribution for the hypothetical case of He atoms forming a strict icosahedral arrangement around the Cs^+ located in the center is included for comparison in the red dashed line.

both the DMC and the classical BH methods. These two approaches yield energies also affected by the intrinsic weakness of the He–Cs$^+$ interaction.

VII. CONCLUSIONS

The solvation of Cs$^+$ ions in helium droplets has been treated in a combined experimental and theoretical investigation. Mass spectra of He$_N$Cs$^+$ clusters up to $N = 60$ were measured, and their abundances have been analyzed as a function of the number of helium atoms in order to search for the most stable cases. Evidences of the closure of the first solvation layer when 17 He atoms surrounding the ion impurity have been presented with the ratio between satellite and main peaks existing in the measured spectra, the former being the result of a fragmentation process in the acceleration region of the mass spectrometer. Calculations performed by means of basin-hopping, diffusion Monte Carlo, and path integral Monte Carlo methods also yield results indicating interesting features for $N = 12$ and $N = 17$. In particular, quantum mechanical distributions for He$_{12}$Cs$^+$ suggest the contribution from the icosahedral configuration and conclusive evidences showing that beyond He$_{17}$Cs$^+$, He atoms are located surrounding the first solvation layer have been given.

ACKNOWLEDGMENTS

REFERENCES

[1] M. Hartmann, R. E. Miller, J. P. Toennies, and A. F. Vilesov, Science **272**, 1631 (1996).

[2] J. P. Toennies and A. F. Vilesov, Annu. Rev. Phys. Chem. **49**, 1 (1998).

[3] S. Yang and A. M. Ellis, Chem. Soc. Rev. **42**, 472 (2013).

[4] C. Callegari, K. K. Lehmann, R. Schmied, and G. Scoles, J. Chem. Phys. **115**, 10090 (2001).

[5] F. Stienkemeier and K. K. Lehmann, J. Phys. B: At., Mol. Opt. Phys. **39**, R127 (2006).

[6] M. Y. Choi, G. E. Douberly, T. M. Falconer, W. K. Lewis, C. M. Lindsay, J. M. Merritt, P. L. Stiles, and R. E. Miller, Int. Rev. Phys. Chem. **25**, 15 (2006).

[7] K. Szalewicz, Int. Rev. Phys. Chem. **27**, 273 (2008).

[8] E. Coccia, E. Bodo, F. Marinetti, F. A. Gianturco, E. Yildrim, M. Yurtsever, and E. Yurtsever, J. Chem. Phys. **126**, 124319 (2007).

[9] L. An der Lan, P. Bartl, C. Leidlmair, R. Jochum, S. Denifl, O. Echt, and P. Scheier, Chem. - Eur. J. **18**, 4411 (2012).

[10] P. Bartl, C. Leidlmair, S. Denifl, P. Scheier, and O. Echt, J. Phys. Chem. A **118**, 8050 (2013).

[11] C. Di Paola, F. Sebastianelli, E. Bodo, I. Baccarelli, and F. A. Gianturco, J. Chem. Theory Comput. **1**, 1045 (2005).

[12] D. E. Galli, M. Buzzacchi, and L. Reatto, J. Chem. Phys. **115**, 10239 (2001).

[13] N. Issaoui, K. Abdessalem, H. Ghalla, S. J. Yaghmour, F. Calvo, and B. Oujia, J. Chem. Phys. **141**, 174316 (2014).

[14] J. H. Kim, D. S. Peterka, C. C. Wang, and D. M. Neumark, J. Chem. Phys. **124**, 214301 (2006).

[15] A. Nakayama and K. Yamashita, J. Chem. Phys. **112**, 10966 (2000).

[16] A. Nakayama and K. Yamashita, J. Chem. Phys. **114**, 780 (2001).

[17] J. V. Pototschnig, F. Lackner, A. W. Hauser, and W. E. Ernst, Phys. Chem. Chem. Phys. **19**, 14718 (2017).

[18] F. Sebastianelli, E. Bodo, I. Baccarelli, C. Di Paola, F. A. Gianturco, and M. Yurtsever, Comput. Mater. Sci. **35**, 261 (2006).

[19] M. Theisen, F. Lackner, and W. E. Ernst, Phys. Chem. Chem. Phys. **12**, 14861 (2010).

[20] M. Theisen, F. Lackner, and W. E. Ernst, J. Chem. Phys. **135**, 074306 (2011).

[21] J. Tiggesbaumker and F. Stienkemeier, Phys. Chem. Chem. Phys. **9**, 4748 (2007).

[22] E. Yurtsever, E. Yildirim, M. Yurtsever, E. Bodo, and F. A. Gianturco, Eur. Phys. J. D **43**, 105 (2007).

[23] A. Mauracher, O. Echt, A. M. Ellis, S. Yang, D. K. Bohme, J. Postler, S. Kaiser, S. Denifl, and P. Scheier, Phys. Rep. **751**, 1 (2018).

[24] M. Mudrich and F. Stienkemeier, Int. Rev. Phys. Chem. **33**, 301 (2014).

[25] S. Müller, M. Mudrich, and F. Stienkemeier, J. Chem. Phys. **131**, 044319 (2009).

[26] M. Rossi, M. Verona, D. E. Galli, and L. Reatto, Phys. Rev. B **69**, 212510 (2004).

[27] F. Marinetti, E. Coccia, F. A. Gianturco, E. Yurtsever, M. Yurtsever, and E. Yildirim, Theor. Chem. Acc. **118**, 53 (2007).

[28] M. Buzzacchi, D. E. Galli, and L. Reatto, Phys. Rev. B **64**, 094512 (2001).

[29] D. E. Galli, D. M. Ceperley, and L. Reatto, J. Phys. Chem. A **115**, 7300 (2011).

[30] L. Kranabetter, M. Goulart, A. Aleem, T. Kurzthaler, M. Kuhn, E. Barwa, M. Renzler, L. Grubweiser, M. Schwärzler, A. Kaiser et al., J. Phys. Chem. C **121**, 10887 (2017).

[31] M. Rastogi, C. Leidlmair, L. An der Lan, J. Ortiz de Zárate, R. Pérez de Tudela, M. Bartolomei, M. I. Hernández, J. Campos-Martínez, T. González-Lezana, J. Hernández-Rojas et al., Phys. Chem. Chem. Phys. **20**, 25569 (2018).

[32] L. F. Gomez, E. Loginov, R. Sliter, and A. F. Vilesov, J. Chem. Phys. **135**, 154201 (2011).

[33] L. An der Lan, P. Bartl, C. Leidlmair, H. Schöbel, R. Jochum, S. Denifl, T. D. Märk, A. M. Ellis, and P. Scheier, J. Chem. Phys. **135**, 044309 (2011).

[34] S. Ralser, J. Postler, M. Harnisch, A. M. Ellis, and P. Scheier, Int. J. Mass Spectrom. **379**, 194 (2015).

[35] R. A. Aziz and M. J. Slaman, J. Chem. Phys. **94**, 8047 (1991).

[36] R. A. Kendall, T. H. Dunning, and R. J. Harrison, J. Chem. Phys. **96**, 6796 (1992).

[37] F. Weigend, Phys. Chem. Chem. Phys. **8**, 1057 (2006).

[38] H. J. Werner, P. J. Knowles, R. Lindh, F. R. Manby, M. Schütz et al., MOLPRO, version 2012.1, a package of ab initio programs, 2012, see http://www.molpro.net/.

[39] F. Pirani, S. Brizi, L. Roncaratti, P. Casavecchia, D. Cappelletti, and F. Vecchiocattivi, Phys. Chem. Chem. Phys. **10**, 5489 (2008).

[40] D. J. Wales and J. P. K. Doye, J. Phys. Chem. A **101**, 5111 (1997).

[41] Z. Li and H. A. Scheraga, Proc. Natl. Acad. Sci. U. S. A **84**, 6611 (1987).

[42] J. Hernández-Rojas, F. Calvo, J. Bretón, and J. Gomez Llorente, J. Phys. Chem. C **116**, 17019 (2012).

[43] S. Acosta-Gutiérrez, J. Bretón, J. Hernández-Rojas, and J. J. Gomez Llorente, J. Chem. Phys. **137**, 074306 (2012).

[44] J. Hernández-Rojas, J. Bretón, J. M. Gomez Llorente, and D. J. Wales, J. Phys. Chem. B **110**, 13357 (2006).

[45] J. P. K. Doye and D. J. Wales, Phys. Rev. B **59**, 2292 (1999).

[46] J. Hernández-Rojas and D. J. Wales, J. Chem. Phys. **119**, 7800 (2003).

[47] T. James, D. J. Wales, and J. Hernández-Rojas, Chem. Phys. Lett. **415**, 302 (2005).

[48] J. Hernández-Rojas, J. Bretón, J. M. Gomez Llorente, and D. J. Wales, J. Chem. Phys. **121**, 12315 (2004).

[49] J. Hernández-Rojas, F. Calvo, F. Rabilloud, J. Bretón, and J. M. Gomez Llorente, J. Phys. Chem. A **114**, 7267 (2010).

[50] D. J. Wales, Energy Landscapes (Cambridge University Press, Cambridge, 2003).

[51] R. Rodríguez-Cantano, R. Pérez de Tudela, M. Bartolomei, M. I. Hernández, J. Campos-Martínez, T. González-Lezana, P. Villarreal, J. Hernández-Rojas, and J. Bretón, J. Chem. Phys. **143**, 224306 (2015).

[52] M. Bartolomei, R. Pérez de Tudela, K. Arteaga, T. González-Lezana, M. I. Hernández, J. Campos-Martínez, P. Villarreal, J. Hernández-Rojas, J. Bretón, and F. Pirani, Phys. Chem. Chem. Phys. **19**, 26358 (2017).

[53] V. Buch, J. Chem. Phys. **97**, 726 (1992).

[54] P. Sandler and V. Buch, Prog. QCLUSTER, private communication, 1999, Vol. 5.

[55] R. Rodríguez-Cantano, T. González-Lezana, P. Villarreal, D. López-Durán, F. A. Gianturco, and G. Delgado-Barrio, Int. J. Quantum Chem. **114**, 1318 (2014).

[56] R. Rodríguez-Cantano, T. González-Lezana, P. Villarreal, and F. A. Gianturco, J. Chem. Phys. **142**, 104303 (2015).

[57] R. Rodríguez-Cantano, T. González-Lezana, and P. Villarreal, Int. Rev. Phys. Chem. **35**, 37 (2016).

[58] R. Rodríguez-Cantano, M. Bartolomei, M. I. Hernández, J. Campos-Martínez, T. González-Lezana, P. Villarreal, R. Pérez de Tudela, F. Pirani, J. Hernández-Rojas, and J. Bretón, J. Chem. Phys. **146**, 034302 (2017).

[59] M. F. Herman, E. J. Bruskin, and B. J. Berne, J. Chem. Phys. **76**, 5150 (1982).

[60] K. R. Glaesemann and L. E. Fried, J. Chem. Phys. **116**, 5951 (2002).

[61] F. Calvo, J. Phys. Chem. A **119**, 5959 (2015).

[62] M. Sprik, M. L. Klein, and D. Chandler, Phys. Rev. B **31**, 4234 (1985).

[63] U. Boesl, Mass Spectrom. Rev. **36**, 86 (2017).

[64] D. Mateo and J. Eloranta, J. Phys. Chem. A **118**, 6407 (2014).

[65] J. I. Martínez and J. A. Alonso, Phys. Chem. Chem. Phys. **20**, 27368 (2018).